iMC-OpenFOAM Coupled Analysis of Passively-Cooled Molten Salt Fast Reactor

Inyup Kim, Yonghee Kim*

Department of Nuclear & Quantum Engineering, Korea Advanced Institute of Science and Technology, 291

Daehak-ro Yuseong-gu, Daejeon, Korea, 34141

*Corresponding author: yongheekim@kaist.ac.kr

*Keywords: iMC, OpenFOAM, Multiphysics, MSR, PMFR

1. Introduction

Molten Salt Reactor (MSR) is one of the advanced reactor concepts which utilizes a liquid molten salt as a fuel. The molten salt reactor is gaining attention due to its inherent safety, accident tolerance, and flexible reactor operation with refueling and removal.

Because of the liquid fuel, analyzing MSRs is a primary research challenge. In terms of neutronics, the delayed neutron precursors may shift and affect the fission chain. Moreover, the molten salt fuel density is dependent on its temperature, which is not found in the solid fuel. This requires the consideration of the density change.

Passive Safety Molten Salt Fast Reactor (PMFR) [1] is a reactor concept suggested by i-SAFE-MSR research center, Republic of Korea. The PMFR is a fast-spectrum reactor utilizing natural circulation. Its design offers advantages in passive safety, prevention of severe accidents, and long operational lifetime.

iMC is a Monte Carlo neutron transport code developed in KAIST [2]. The code is specialized in the MSR analysis, including the delayed neutron precursor tracking [3] and removal/addition of the nuclide during the depletion [4]. OpenFOAM is an open-sourced computational fluid dynamics code [5]. The OpenFOAM is externally coupled with the iMC code to obtain temperature and velocity distribution of the fuel from the heating distribution. The coupled approach with iMC was previously studied with 2-dimensional MSR benchmark [6].

This study covers a multiphysics analysis of the PMFR reactor, using the coupled approach of the iMC and OpenFOAM codes. In addition to the coupled result, this work will highlight key remarks on coupled neutronics—fluid dynamics analysis for MSRs.

2. Methods

This section focuses on the delayed neutron precursor tracking scheme in the iMC code. The detailed explanation on the iMC-OpenFOAM coupling can be found in previous publication [6].

2.1 Coupling scheme

The iMC and OpenFOAM codes are coupled externally, based on the file transfer. The initial iMC analysis is performed, assuming uniform temperature

and static fuel. The static fuel assumption is due to absence of a flow profile. However, the power distribution itself is nearly unaffected by the delayed neutron precursor shift, and the results are coupled with OpenFOAM to obtain a converged solution with Picard iteration..

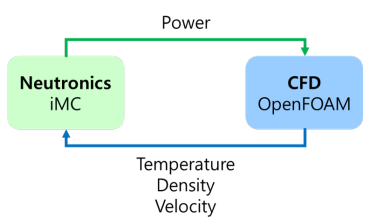


Fig. 1. iMC-OpenFOAM data transfer

2.2 Delayed neutron precursor tracking

The iMC code previously performed studies regarding the precursor tracking on the moving fuel. This study introduces a current precursor tracking scheme implemented in the iMC code.

For static reactor, a balance equation for the delayed neutron precursor with precursor group i can be expressed as below:

$$\frac{dC_i}{dt} = -\lambda_i C_i + \beta_i \nu \Sigma_f \phi \tag{1}$$

where λ_i , C_i , β_i are decay constant, precursor concentration, and delayed neutron fraction of the group i. The term $\nu \Sigma_f \phi$ denotes a fission rate. The Eq. (1) results in a steady-state solution C_i and delayed neutron production of:

$$C_i = \frac{\beta_i}{\lambda_i} \nu \Sigma_f \phi \to \lambda_i C_i = \beta_i \nu \Sigma_f \phi. \tag{2}$$

This implies that delayed neutron precursor production can be evaluated without sampling birth and decay of the precursors.

However, the Eq. (1) can be re-written with consideration of the fuel flow profile \vec{U} :

$$\frac{dC_i}{dt} + \vec{U} \cdot \nabla C_i = -\lambda_i C_i + \beta_i \nu \Sigma_f \phi \tag{3}$$

The solution cannot be found analytically, since the flow profile is often given with finite volume-wise. Instead, in accordance with Lagrangian Particle Tracking [7], directly tracking the trajectory of the precursor can find the steady-state solution indirectly. This includes sampling an emission time and tracking the precursor until its decay.

The precursor position is updated based on the emission time and fuel velocity profile. Since the iMC currently couples with the OpenFOAM on a coarser finite-volume grid, the direct particle tracking is conducted within the finite volume. In addition, the inactive region is simplified into 1-dimensional model to avoid tracking of precursors within low-importance region, an inactive core. The out-of-core is lumped into an 1-dimensional extension, with uniform velocity. When the precursor reaches the top of the active core, it is assumed to travel through the extension, and re-enter if possible.

Regarding the re-entering precursors, previous method simply uniformly distributed the precursors. However, the approach is far from the realistic, especially for the PMFR. Currently, the iMC code pre-calculates the finite volume-wise mass flow. The mass flow is then normalized to act as a probability density for each finite volume, as in Eq. (4).

$$p_i = \frac{\dot{m}_i}{\sum_{j=core\ bottom} \dot{m}_j} \tag{4}$$

 \dot{m} denotes a mass flow of finite volume and subscript stands for the finite volume index. With probability p_i , the precursor re-enters to the finite volume i. The approach is identical to the previous, if the inlet mass flow is uniform. However, in the PMFR, the flow is not uniform, due to structure below the active core.

3. Numerical Results

3.1 Model description

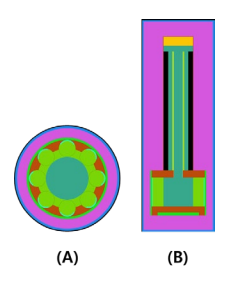


Fig. 2. Cross-sectional (A) and side view (B) of the PMFR reactor model

Figure 2 is a cross-sectional and side view of the PMFR reactor. The active core, where coupling with the OpenFOAM is conducted, is depicted in the side view. The active core is a cylinder with radius of 100 cm and height of 195 cm. Note that the burnable absorber is excluded for convenient modeling, which leads to a higher reactivity compared to previous studies [1].

The fuel is NaCl-KCl-UCl3, using HALEU with enrichment of 19.75 weight-%. Density of the fuel is assumed as follows:

$$\rho_{fuel}[g/cm^3] = 4.315326 - 0.001092 T_{fuel}[K].$$
 (5)

where ρ_{fuel} and T_{fuel} are density and temperature of the fuel salt.

The reactor comprises stainless steel as a structural material, B₄C as a shielding, and BeO as a reflector. The model contains control drum, with all drums heading out.

The iMC code performs a neutron-photon coupled transport to obtain accurate power distribution. The calculation is performed with ENDF-B/VII.1 neutron cross-section [8], MCPLIB84 photon cross-section libraries [9]. The neutronics calculation is conducted with 100,000 histories per cycle with 200 inactive, and 500 active cycles. This analysis results in a standard deviation of k_{eff} around 8 pcm.

Neutronics tally grid and fluid dynamics grid are equivalent: 5 cm radial and 5 cm axial sized mesh. The mesh subdivides the active core into 20 radial and 39 axial meshes. The temperature change is considered based on GHQ Doppler broadening [10], and the density change is handled with relative density at 923 K. The iterative fission probability (IFP) is applied with 15 latent cycles to obtain an effective kinetic parameters [11]. The residual time of the reactor is assumed to be 20 seconds.

OpenFOAM *buoyantSimpleFoam* solver is utilized to solve the steady-state behavior for the power distribution from the iMC calculation. For initial coupling, 850,000 timesteps are used to obtain fully converged solution. From the next iteration step, 5,000 timesteps are used for updated power distribution, starting from the previous iteration solution. No relaxation is applied to the coupled analysis.

The iteration first performs neutronics analysis with a uniform temperature of 923.0 K. The power distribution is processed in OpenFOAM to produce the initial temperature and density distribution of the iMC analysis.

3.2. Result

Figure 3 is an evolution of k_{eff} and total β_{eff} , based on the IFP, by iteration number with 2-sigma error bars. The figure shows that the coupled result converges within few iterations. The plot also shows that the effective delayed neutron fraction, which reflects the impact of the velocity profile, converges quickly, while the temperature profile requires more iterations.

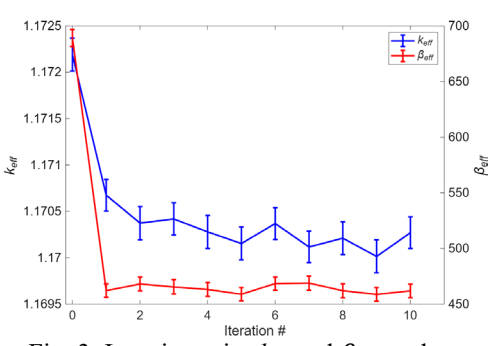


Fig. 3. Iteration-wise k_{eff} and β_{eff} values

Table I compares the initial and last effective delayed neutron fraction of each delayed neutron group. Note that lower group indices correspond to longer half-lives. Over 50 % of precursors of groups 1 to 3 escape from the active core. In contrast, precursors in groups with shorter half-lives rarely escape the core because of their shorter emission times.

Table I. Effective delayed neutron fractions for initial and last iteration steps

$oldsymbol{eta}_{eff}$	Initial [pcm]	10 th iteration [pcm]	Reduction [pcm (%)]
Group 1	22.0 ± 0.6	8.2 ± 0.4	-13.7 (-62%)
Group 2	114.4 ± 1.5	47.0 ± 0.8	-67.3 (-58%)
Group 3	110.5 ± 1.4	53.5 ± 0.9	-57.0 (-51%)
Group 4	266.7 ± 2.2	191.3 ± 1.9	-75.3 (-28%)
Group 5	122.2 ± 1.4	110.6 ± 1.4	-11.6 (-9%)
Group 6	52.9 ± 1.0	50.9 ± 0.9	-2.0 (-3%)
Total	689.0 ± 3.7	461.8 ± 3.0	-227 (-32%)

Figure 4 shows active core power and neutron flux distributions in radial and axial directions. The quantities are tallied in the last iteration step. The core peripheral region is locally heated, due to existence of the reflector. This behavior produces a high-temperature region in the upper-right corner of Figure 5. The center and right panels of Figure 5 show fuel speed and velocity.

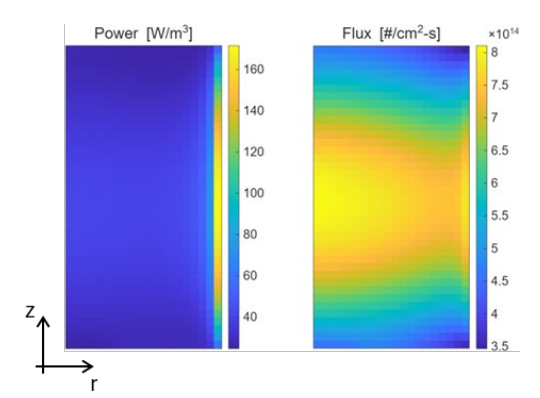


Fig. 4. Power and neutron flux distribution

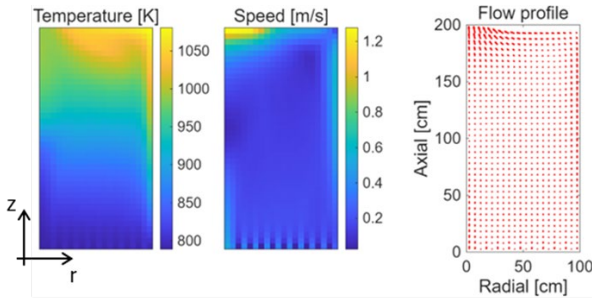


Fig. 5. Temperature (left), fuel speed (center), and velocity field (right).

3.3. Sensitivity Analysis

The impact of the delayed neutron precursor tracking is studied using the last iteration step's temperature and density distribution, with and without the velocity field. Figures 6 and 7 show distributions of the delayed neutrons in static and flowing fuel. For the static fuel, the delayed neutron distribution nearly follows the power distribution. However, the flowing fuel is shifted upwards. Table II shows a comparison of reactor parameters: k_{eff} and β_{eff} of two cases. Note that the converged state from Section 3.2 is utilized for Table II.

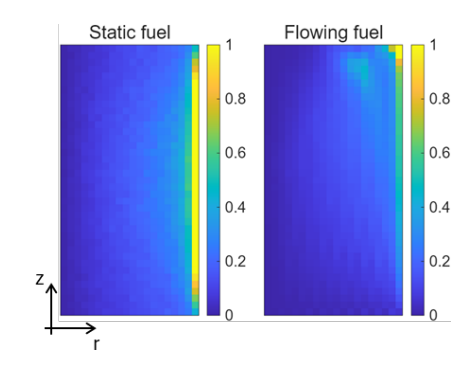


Fig. 6. Distribution of delayed neutrons

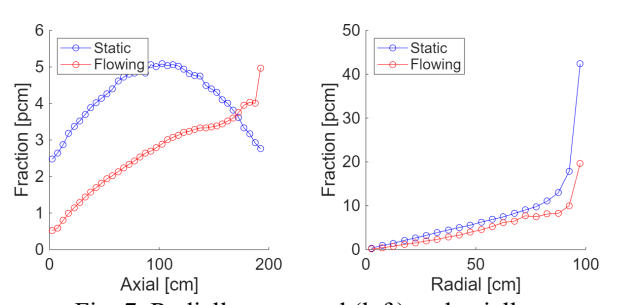


Fig. 7. Radially-averaged (left) and axially-averaged(right) delayed neutron distribution

Table II. Comparison between static and flowing cases

Cases	k_{eff}	β _{eff} [pcm]
Static	1.173057 ± 8.6	697.5 ± 3.5
Flowing	1.170269 ± 8.5	461.8 ± 3.0
Difference [pcm]	-278.8 ± 12.1	-235.7 ± 4.6

As mentioned earlier, temperature contribution can be subdivided between Doppler broadening and density change. Regarding the uniform temperature and density, an initial condition 923.0 K and corresponding density were utilized. Table III compares the reactivity contribution of the temperature and density field applied. Figure 8 plots a relative difference in power distribution with uniform temperature and density applied. The comparison clearly shows that the temperature contribution on the power distribution and multiplication factor is higher than the density change. Nevertheless, the density distribution has non-negligible impact on the reactor performance.

Table III. Reactivity change from temperature (T) and density (ρ) fields

$\Delta \rho$ [pcm]	Uniform T	T distribution
Uniform $ ho$	-	-162 ± 12
ρ distribution	-1222 ± 12	-1386 ± 12

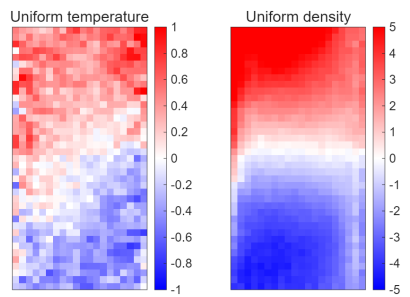


Fig. 8. Relative difference in power distributions [%] for uniform temperature and density.

The iMC code supports both sole neutron and neutron-photon coupled transport. In addition, the total power may be tallied based on widely-used fission energy release, while this study uses a energy loss per collision. The difference in methodology doesn't affect the reactor parameter such as $k_{\rm eff}$. However, according to Figure 9, the fission energy release overestimates the power distribution. In this reactor, the photon-induced power is roughly 6.7 % of total power. In the coupled neutron-photon transport, heating is leaked to the surrounding structure of the active core, which leads to lower power at the peripheral region compared to the fission energy release.

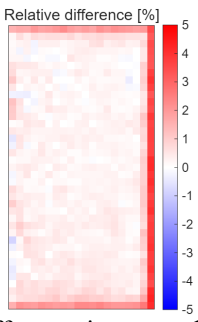


Fig. 9. Relative difference in power distribution for sole neutron and neutron-photon coupled transports.

4. Conclusions

In this research, the neutronics-fluid dynamics coupled analysis is conducted by coupling iMC Monte Carlo and OpenFOAM CFD codes. The study covers the coupling scheme, with emphasis on the delayed neutron tracking scheme. The multiphysics approach is applied to the PMFR model and showed converged behavior. Several sensitivity studies highlight the importance of parameters such as fuel density and delayed neutron precursor shift. These effects are negligible in conventional solid-fuel reactors but are critical in MSRs.

In the current scheme, most neutronics analyses focus on the active core fuel, which is a major contribution to the reactor performance. However, the analysis requires sensitivity studies on these assumptions. With the introduction of neutron-photon transport, structural heating can also be analyzed. Given the peripheral region's importance in this reactor, temperature changes are expected to have a non-negligible impact on the coupling.

Acknowledgement

This work was supported by the National Research Foundation of Korea (NRF) Grant funded by the Korean Government (MSIP) (2021M2D2A2076383).

REFERENCES

- [1] Aufanni, N. N., Lee, E., Oh, T., & Kim, Y. (2024). Burnable absorber design study for a passively-cooled molten salt fast reactor. Nuclear Engineering and Technology, 56(3), 900–906. https://doi.org/10.1016/j.net.2023.11.001
- [2] Kim, H., and Kim, Y. (2021). Unstructured mesh-based neutronics and thermomechanics coupled steady-state analysis on advanced three-dimensional fuel elements with Monte Carlo Code iMC. Nucl. Sci. Eng. 195 (5), 464–477. doi:10.1080/00295639.2020.1839342
- [3] Kim, I., Oh, T., and Kim, Y. (2024). "Development of a delayed neutron precursor tracking module for molten salt reactors in the iMC Monte Carlo code," in Proceedings of the International Conference on Physics of Reactors, PHYSOR 2024, San Francisco, United States, 21 Apr 2024-24 Apr 2024. [4] Kim, I., Oh, T., and Kim, Y. (2025). Development and verification of depletion capabilities in the iMC Monte Carlo code. Ann. Nucl. Energy 216, 111260. doi:10.1016/j.anucene.2025.111260
- [5] Weller, H. G., Tabor, G., Jasak, H., and Fureby, C. (1998). A tensorial approach to computational continuum mechanics using object-oriented techniques. Comput. Phys. 12 (6), 620–631. doi:10.1063/1.168744
- [6] Kim, I., Oh, T., & Kim, Y. (2025). Coupling of the Monte Carlo IMC and openfoam codes for multiphysics calculations of molten salt reactors. Frontiers in Nuclear Engineering, 4. https://doi.org/10.3389/fnuen.2025.1595628
- [7] Schroeder, A., Schanz, D. (2023). 3D Lagrangian Particle Tracking in Fluid Mechanics, Annual Review of Fluid Mechanics, Vol. 55. https://doi.org/10.1146/annurev-fluid-031822-041721
- [8] Chadwick, M. B., Herman, M., Oblozinsky, P., Dunn, M., Danon, Y., Kahler, A., et al. (2011). ENDF/B-VII.1 nuclear data for science and technology: cross sections, covariances, fission product yields and decay data. Nucl. Data Sheets 112 (12), 2887–2996.
- [9] White, M. C., (2012). Further Notes on MCPLIB03/04 and New MCPLIB63/84 Compton Broadening Data For All Versions of MCNP5, LA-UR-12-00018.
- [10] Jo, Y. G., Cho, N. Z., (2017). Refinements of On-The-Fly Doppler Broadening via Gauss-Hermite Quadrature in Monte Carlo Reactor Analysis, Transactions of the Korean Nuclear Society Spring Meeting, Jeju, Republic of Korea.
- [11] Oh, T., Kim, I., Kim, Y. (2025). Evaluation of effective kinetic parameters and adjoint flux distribution using iterated fission probability in the iMC Monte Carlo code, Annals of Nuclear Energy, Vol. 210. https://doi.org/10.1016/j.anucene.2024.110878